

Evolution of Urca Pairs in the Crusts of Highly Magnetized Neutron Stars

MICHAEL A. FAMIANO,^{1,2,3} GRANT MATHEWS,^{3,4} A. BAHA BALANTEKIN,^{2,5} TOSHITAKA KAJINO,^{6,2,7}
MOTOHIKO KUSAKABE,⁶ AND KANJI MORI⁸

¹Western Michigan University, Kalamazoo, MI 49008-5252 USA

²National Astronomical Observatory of Japan, 2-21-1 Osawa, Mitaka, Tokyo 181-8588 Japan

³Joint Institute for Nuclear Astrophysics - Center for the Evolution of the Elements, USA

⁴Center for Astrophysics, Department of Physics and Astronomy, University of Notre Dame, Notre Dame, IN 46556, USA

⁵Department of Physics, University of Wisconsin-Madison, Madison, Wisconsin 53706 USA

⁶School of Physics, Beihang University, 37 Xueyuan Road, Haidian-qu, Beijing 100083, China

⁷Graduate School of Science, The University of Tokyo, 7-3-1 Hongo, Bunkyo-ku, Tokyo, 113-0033 Japan

⁸Research Institute of Stellar Explosive Phenomena, Fukuoka University,
8-19-1 Nanakuma, Jonan-ku, Fukuoka-shi, Fukuoka 814-0180, Japan

ABSTRACT

We report on the effects of strong magnetic fields on neutrino emission in the modified Urca process. We show that the effect of Landau levels on the various Urca pairs affects the neutrino emission spectrum and leads to an angular asymmetry in the neutrino emission. For low magnetic fields the Landau levels have almost no effect on the cooling. However, as the field strength increases, the electron chemical potential increases resulting in a lower density at which Urca pairs can exist. For intermediate field strength there is an interesting interference between the Landau level distribution and the Fermi distribution. For high enough field strength, the entire electron energy spectrum is eventually confined to single Landau level producing dramatic spikes in the emission spectrum.

Keywords: PPISN – PISN – black holes – massive stars – nuclear physics

1. INTRODUCTION

It is by now widely accepted that soft gamma-ray repeaters (SGRs) and anomalous X-ray pulsars (AXPs) correspond to a class of neutron stars known as magnetars. These objects are warm, isolated, and slowly rotating neutron stars of age $\sim 10^5$ yr with unusually strong surface magnetic fields. Indeed, both pulsars and magnetars have strong magnetic fields at their surface that can be as large as 10^{12} to 10^{16} G (Kouveliotou et al. 1998; Turolla et al. 2015). Moreover, the interior field can be as large as the equipartition limit of order 10^{18} G (Lai et al. 1991; Chanmugam 1992).

Among possible explanations for the cooling of magnetars, decay processes leading to neutrino or anti-neutrino emission such as the direct Urca (DU) process ($n \rightarrow p + e^- + \bar{\nu}_e$, $p + e^- \rightarrow n + \nu_e$), the modified Urca (MU) process ($n + N \rightarrow p + e^- + N' + \bar{\nu}_e$, $p + e^- + N \rightarrow n + N' + \nu_e$) (Haensel & Gnedin 1994; Yakovlev & Levenfish 1995; Yakovlev et al. 2001), or the neutrino-pair emission process ($N_1 + N_2 \rightarrow N'_1 + N'_2 + \nu + \bar{\nu}$) are possible.

Early in the cooling process the DU process is a viable candidate to explain the rapid cooling of NSs (Boguta 1981; Lattimer et al. 1991; Maruyama et al. 2022). However, in this paper we are more concerned with the MU process.

michael.famiano@wmich.edu

gmathews@nd.edu

baha@physics.wisc.edu

kajino@buaa.edu.cn

kusakabe@buaa.edu.cn

kanji.mori@fukuoka-u.ac.jp

The DU process takes place at high temperature and density and for certain ratios of constituents. However, under less extreme conditions when the DU process is diminished, the MU process can continue to occur.

In particular, the Urca cycles of electron capture and β decay on pair nuclei at a depth of about 150 m in neutron stars were shown to occur in [Schatz et al. \(2014\)](#) although this mechanism had been previously discussed in the context of white dwarfs ([Tsuruta & Cameron 1970](#)), Type Ia supernovae ([Paczyński 1972](#); [Woosley & Weaver 1986](#)) and electron-degenerate supernovae ([Jones et al. 2013](#)). The Urca cycle operates to cool the outer neutron star crust by emitting neutrinos while also thermally decoupling the surface layers from the deeper crust. This cooling eliminates the possibility that interior heating produces the unexpectedly short recurrence times of energetic thermonuclear bursts on neutron stars. The Urca cycles also indicate that the ignition scenario of superbursts by $^{12}\text{C}+^{12}\text{C}$ fusion reaction, whose reaction rate is severely limited in recent theoretical studies ([Mori et al. 2019](#)), would require another heat source because of higher neutrino emissivity for cooling.

In previous studies, however, the effects of possible strong magnetic fields on the modified Urca process have not been considered. Here we show that the appearance of Landau levels for electrons experiencing strong magnetic fields significantly alters the operation of the various Urca pairs proposed by [Schatz et al. \(2014\)](#) and affects the neutrino emission spectrum leading to an angular asymmetry in the neutrino emissivity. For low magnetic fields the Landau levels have almost no effect on the cooling. However, as the field strength increases, the electron chemical potential increases resulting in a lower density at which Urca pairs can exist. For intermediate field strength there is an interesting interference between the Landau level distribution and the Fermi distribution. For high enough field strength, eventually the entire electron energy spectrum is confined to single Landau level producing dramatic spikes in the emission spectrum.

This paper is organized as follows: The ingredients of the model for the MU are summarized in Section 2. The results are presented in Section 3. Our discussion and conclusions are in Section 4.

2. THE MODEL

2.1. Weak Interaction Rates in External Fields

In a homogeneous plasma at a given temperature and density, the electron chemical potential will change in the presence of a strong magnetic field. This will ultimately change the effectiveness of a particular Urca pair for a given environment. If a dipole field is assumed, then the electron chemical potential, which depends on the magnetic field, will in turn depend on the angular position with respect to the magnetic pole for a constant density and temperature within the crust. The electron number density with the electron transverse momentum components constrained to Landau levels is ([Famiano et al. 2020](#); [Grasso & Rubinstein 2001](#); [Kawasaki & Kusakabe 2012](#)):

$$\begin{aligned} n_e = n_- - n_+ &= \frac{1}{4\pi^2} \int_0^\infty d^3p \left(\left[\exp\left(\frac{E-\mu}{T}\right) + 1 \right]^{-1} - \left[\exp\left(\frac{E+\mu}{T}\right) + 1 \right]^{-1} \right) \\ &= \int_0^\infty dp_x dp_y dp_z \left(\left[\exp\left(\frac{E-\mu}{T}\right) + 1 \right]^{-1} - \left[\exp\left(\frac{E+\mu}{T}\right) + 1 \right]^{-1} \right) \\ &= \frac{eB}{2\pi^2} \sum_{n=0}^\infty g_n \int_0^\infty dp_z \left(\left[\exp\left(\frac{\sqrt{p_z^2 + m_e^2 + 2neB} - \mu}{T}\right) + 1 \right]^{-1} \right. \\ &\quad \left. - \left[\exp\left(\frac{\sqrt{p_z^2 + m_e^2 + 2neB} + \mu}{T}\right) + 1 \right]^{-1} \right) \end{aligned} \quad (1)$$

where g_n is the degeneracy of individual Landau levels n :

$$g_n = \begin{cases} 1, & n = 0 \\ 2, & n > 0 \end{cases}. \quad (2)$$

Natural units are used in this manuscript ($k = \hbar = c = 1$).

Weak interaction rates are computed as in [Famiano et al. \(2020\)](#) and [Arcones et al. \(2010\)](#). In the presence of an external field, the electron energy density is reconfigured by the presence of the field such that the components of the electron momentum perpendicular to the external magnetic field, $p_\perp^2 = p_x^2 + p_y^2$, are placed into individual levels, $p_{\perp,n}^2 = neB$. This quantization results in a shift in the electron chemical potential, μ_e , and ultimately the weak

interaction rates (Luo et al. 2020; Grasso & Rubinstein 2001; Fassio-Canuto 1969). At low fields, $B \lesssim B_c$, where $B_c \sim m_e^2/e = 4.4 \times 10^{13}$ G, the Fermi distribution of the electrons is very similar to the distribution in which $B=0$. In this region, the spacing between individual Landau levels is small, and the phase space distributions in Equation (1) between the magnetized plasma and the non-magnetized plasma are similar (Luo et al. 2020; Grasso & Rubinstein 2001; Fassio-Canuto 1969):

$$dn \propto \frac{d^3p}{(2\pi)^3} = \sum_{n=0}^{\infty} (2 - \delta_{n0}) \frac{eB}{2\pi^2} dp_z. \quad (3)$$

From this, the Fermi-Dirac distribution for the n^{th} Landau level is rewritten:

$$f_{FD}(E, \mu_e) = \frac{1}{\exp\left[\frac{\sqrt{E^2 + 2neB} - \mu_e}{T}\right] + 1}. \quad (4)$$

Following the prescription of Arcones et al. (2010) and Famiano et al. (2020), the weak interaction rates are approximated as:

$$\Gamma_{\beta^-} = \kappa \frac{eB}{2} \sum_{n=0}^{N_{max}} (2 - \delta_{n0}) \int_{\omega_{\beta}}^Q \frac{E(Q-E)^2}{\sqrt{E^2 - m_e^2 - 2neB}} (1 - f_{FD}(E, \mu_e)) (1 - f_{FD}(Q-E, -\mu_{\nu})) dE, \quad (5)$$

$$\Gamma_{\beta^+} = \kappa \frac{eB}{2} \sum_{n=0}^{N_{max}} (2 - \delta_{n0}) \int_{\omega_{\beta}}^{-Q} \frac{E(-Q-E)^2}{\sqrt{E^2 - m_e^2 - 2neB}} (1 - f_{FD}(E, -\mu_e)) (1 - f_{FD}(-Q-E, -\mu_{\nu})) dE, \quad (6)$$

$$\Gamma_{EC} = \kappa \frac{eB}{2} \sum_{n=0}^{N_{max}} (2 - \delta_{n0}) \int_{\omega_{EC}}^{\infty} \frac{E(E-Q)^2}{\sqrt{E^2 - m_e^2 - 2neB}} f_{FD}(E, \mu_e) (1 - f_{FD}(E-Q, \mu_{\nu})) dE, \quad (7)$$

$$\Gamma_{PC} = \kappa \frac{eB}{2} \sum_{n=0}^{N_{max}} (2 - \delta_{n0}) \int_{\omega_{PC}}^{\infty} \frac{E(E+Q)^2}{\sqrt{E^2 - m_e^2 - 2neB}} f_{FD}(E, -\mu_e) (1 - f_{FD}(E+Q, -\mu_{\nu})) dE, \quad (8)$$

in which the following are defined:

$$\begin{aligned} \omega_{EC/PC} &\equiv \max[\pm Q, m_e], \\ \omega_{\beta} &\equiv \sqrt{m_e^2 + 2neB}, \\ N_{max} &\leq \frac{Q^2 - m_e^2}{2eB}, \\ \kappa &\equiv \frac{B \ln 2}{K m_e^5}, \\ B &\equiv 1 + 3g_A^2 = \begin{cases} 5.76, & \text{nucleons,} \\ 4.6, & \text{nuclei,} \end{cases} \\ K &\equiv \frac{2\pi^3 \hbar^7 \ln 2}{G_V^2 m_e^5} = 6144 \text{ s} \end{aligned} \quad (9)$$

and Q is the nuclear mass difference between the parent and daughter nucleus.

In this evaluation, we recognize that the above rates are semi-classical approximations in which nuclear structure and sums over excited states are ignored. We take this approach to examine the overall gross effects of the external field. The rates evaluated above can be adapted to individual sums over individual transitions from parent to daughter states if desired. In this work, we simplify the above to examine ratios of transition rates in an external field to those without a field.

In a charge-neutral plasma at temperature T and electron charge density $\rho Y_e/N_A$, the electron chemical potential is calculated from Eq. (1). The chemical potential is then used in Eqs. (5) – (8) to evaluate the modified rates.

2.2. Urca Pairs

For an Urca pair to exist (Schatz et al. 2014), a pair of nuclei, ${}^A Z$ and ${}^A(Z+1)$ must be linked by weak interactions



The electron energy distribution in the plasma must also be non-degenerate at energies less than the β^- decay Q value and non-zero at energies greater than the electron-capture Q value. In other words, the electron phase space must be simultaneously available for both β^- decays and electron capture. For a plasma in which this condition is met $\mu_e \approx Q_{\beta^-} = -Q_{EC}$. The finite plasma temperature results in the availability of electron states at energies below Q and electrons occupying states at energies above Q. Under these conditions, the Urca pair will undergo captures and decays, resulting in enhanced cooling via neutrino emission. Captures may occur to low-lying states of the daughter nucleus (Schatz et al. 2014).

In the absence of a magnetic field, the electron chemical potential is constrained by the temperature, T , and the charge density ρY_e of the plasma. That is, for a specific temperature, there is only a one-to-one relationship between electron chemical potential and charge density. In fact, there exists a range of charge densities that define an Urca pair because of the finite plasma temperature. The Urca pair is constrained to the region where $Q - kT \lesssim \mu \lesssim Q + kT$. Thus, for a specific temperature, T , and electron chemical potential, μ , a range of densities for which an Urca pair exists can be defined, $\rho Y_e(T, \mu - kT) \lesssim \rho Y_e \lesssim \rho Y_e(T, \mu + kT)$. It has been found (Schatz et al. 2014; Deibel et al. 2016) that this density range results in a thin layer in which a particular pair can exist.

However, this constraining relationship is broken by the introduction of an external magnetic field, $\mu = \mu(T, \rho Y_e, B)$. This may have multiple effects because:

- The electron chemical potential depends on the external field, the density at which an Urca pair forms for a particular temperature changes, resulting in a changed emissivity.
- Weak rates may change at various field strengths, changing the neutrino emissivity.
- For a specific T , ρY_e , and B , new Urca pairs may result from changes in the chemical potential. In addition, existing Urca pairs may be prohibited as the field changes.
- EC rates on excited state nuclei will change with the magnetic field strength. Concurrent changes in the β -decay rates of the daughter nucleus may result in similar rates between excited states and the existence of Urca pairs which involve formerly inaccessible excited states in nuclei.
- For a non-uniform magnetic field on the surface of a highly-magnetized neutron star, the location of Urca pairs in the ocean and crust of a neutron star may depend on the location on the surface of the star.

For a specific Urca pair, the emissivity and luminosity can be calculated following the method of Deibel et al. (2016): Our model for the neutron star and the emissivity in the modified Urca process are directly dependent on the weak interaction rates (Tsuruta & Cameron 1970; Deibel et al. 2016):

$$\epsilon_{\pm} \approx m_e \Gamma_{\pm}. \quad (11)$$

In this work, we define the quantity ϵ_{22} :

$$\epsilon_{22} \equiv \frac{(\epsilon_- + \epsilon_+)}{10^{22}} \quad (12)$$

The geometric thickness of an Urca layer can be shown to be quite thin. In this case, the luminosity (in units of $10^{32} \text{ erg s}^{-1}$ as a function of polar angle, assuming a relativistic correction is:

$$L_{32}(\theta) \equiv \epsilon \times 2\pi R^2 \sin(\theta) \Delta\theta \Delta R / (10^{32} \text{ erg s}^{-1}) \quad (13)$$

The radial thickness of each zone is calculated using the formulation of Schatz et al. (2014) and is found to be $\sim 1 \text{ m}$.

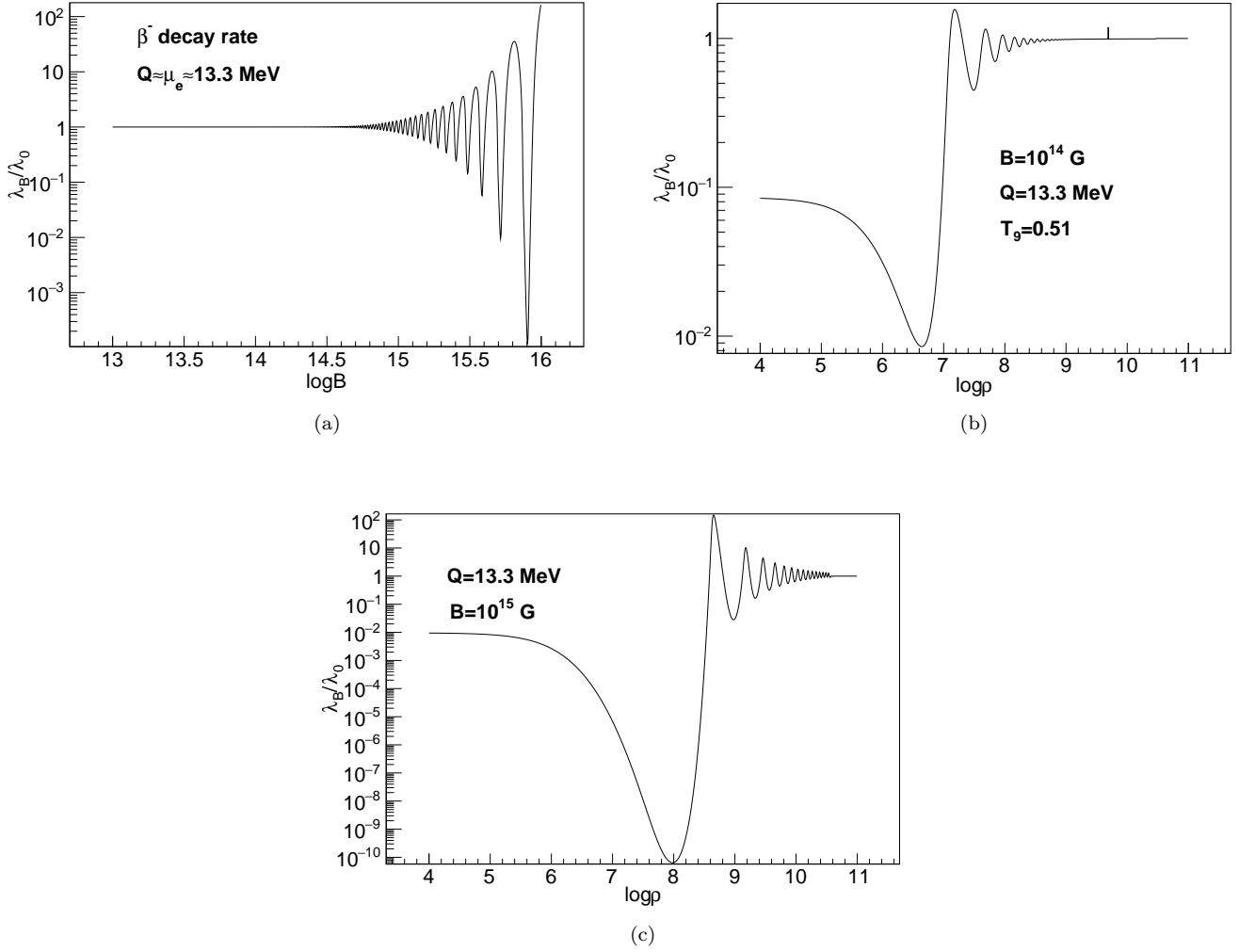


Figure 1. (a) Ratio of β^- decay rates with and without a magnetic field as a function of magnetic field strength for a temperature and ρY_e resulting in an electron chemical potential approximately equal to a Q value of 13.3 MeV. (b) Rate ratio as a function of density for $Y_e=0.5$, $T_9=0.51$, and $B=10^{14}$ G. (c) Rate ratio as a function of density for $Y_e=0.5$, $T_9=0.51$, and $B=10^{15}$ G.

3. RESULTS

The β^- decay rate ratio $\lambda(B)/\lambda(B=0)$ is shown as a function of the magnetic field in Figure 1(a) for $T_9=0.51$, $Y_e=0.5$, and $\rho=4 \times 10^{10}$ g cm $^{-3}$. The oscillations in the decay rate occurs with a change in the field as fewer Landau levels contribute to the electron energy spectrum and as Landau levels shift across the spectrum.

The decay rate ratio as a function of density is shown in Figure 1(b) for $T_9=0.51$ and $B=10^{14}$ G. While the oscillatory behavior of Figure 1(a) can be explained by Landau levels shifting into or out of the electron energy spectrum as the field changes, in Figure 1(b), the oscillatory behavior can be explained by the shift in electron chemical potential as the density increases. The change in chemical potential results in the electron energy spectrum shifting with respect to the existing Landau levels. The same behavior is shown for a field of 10^{15} G in Figure 1(c).

Figure 2 shows the ratio of electron capture rates $\lambda(B)/\lambda(B=0)$ as a function of polar angle about the axis of the neutron star for two different values of field (as indicated at the pole). The field is assumed to be a dipole field. Electron capture rates are computed at the stellar surface. For each case, $Q_{EC} = 5$ MeV. For a weaker field, more Landau levels are present in the electron phase space, and as the field changes across the surface of the star a larger number of Landau levels are shifted out of the electron energy spectrum resulting in the larger number of fluctuations

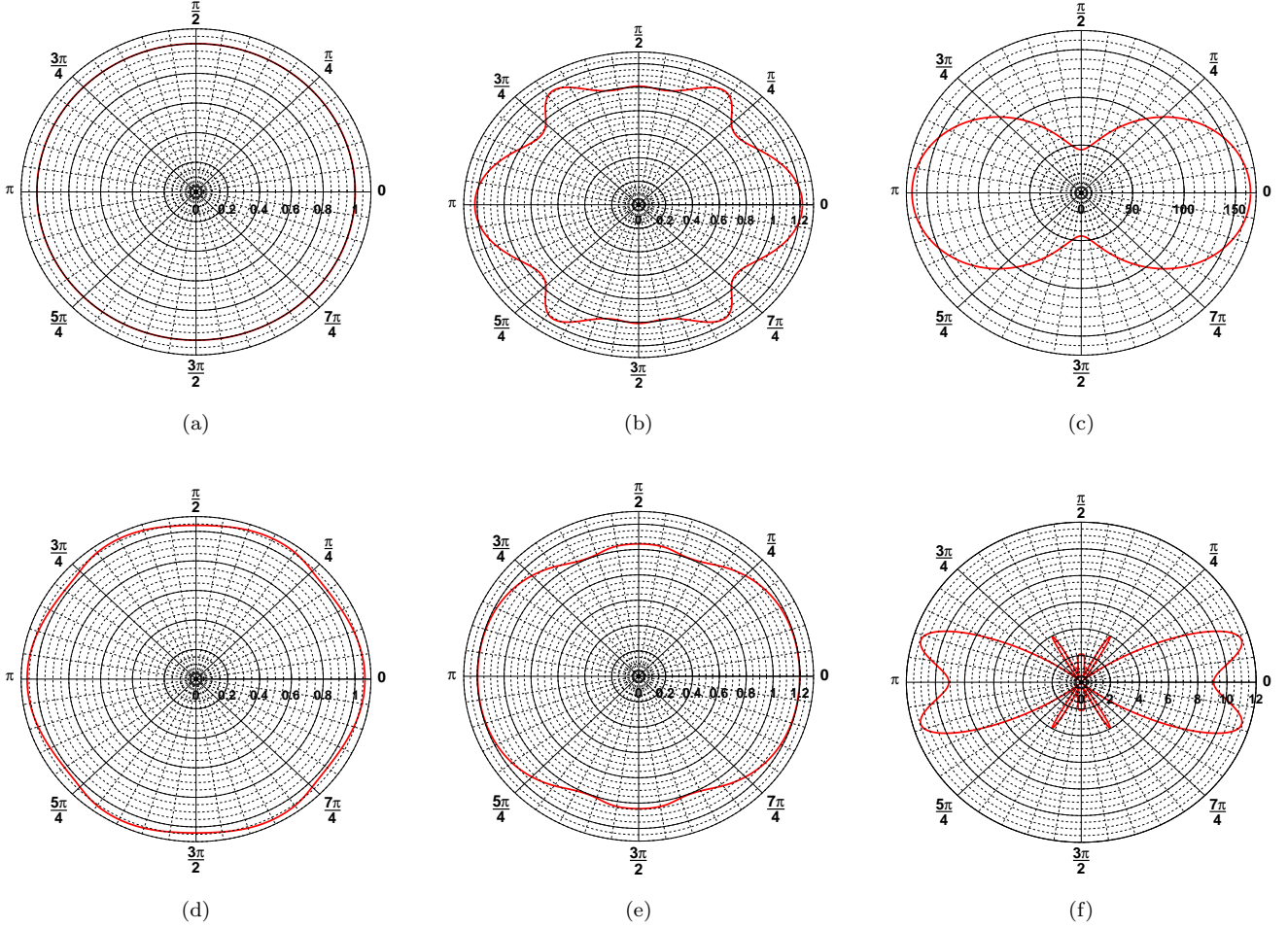


Figure 2. Ratios of β^- decay rates $\lambda(B \neq 0)/\lambda(B = 0)$ as a function of polar angle, θ as measured from a magnetic pole of the star for $Q_{\beta^-} = 5$ MeV. The top row shows the field dependence at a constant $\rho Y_e = 10^9$ g cm $^{-3}$ for (a) $B=10^{14}$ G, (b) $B=10^{15}$ G, and (c) $B=10^{16}$ G. The bottom row shows the sensitivity to density at a constant $B=10^{15}$ G for $\rho Y_e/10^9$ of (d) 0.3 g cm $^{-3}$, (e) 0.6 g cm $^{-3}$, and (f) 2 g cm $^{-3}$.

in the EC rate. However, for a larger field, fewer Landau levels are included in the electron energy spectrum, and as the field shifts across the surface of the star, fewer Landau levels shift into or out of the electron energy spectrum. Thus, there are fewer oscillations in the EC rate across the surface of the star.

In order for efficient Urca pair cooling to occur, EC and β^- decay rates must be similar. We thus examine these rates as a function of magnetic field for several Urca pairs. In Figure 3, rates are shown as a function of magnetic field for two presumed Urca pairs [Schatz et al. \(2014\)](#). In each figure, the black line corresponds to β^- decay rates while the red line corresponds to EC rates. Optimal Urca pair cooling occurs if the rates are similar. However, as the field increases, there can be oscillations in the rates, reducing the efficiency of the associated pair. For example, consider the $^{29}\text{Mg} \leftrightarrow ^{29}\text{Na}$ pair in Figure 3 at the temperature, density, and electron fraction indicated. At a field of $B \approx 10^{15.8}$, the EC rate exceeds the β^- rate by about five orders of magnitude. However, at a field strength slightly lower than this, the rates intersect on the graph. At very high fields, the rates diverge significantly, as only one Landau level contributes to the electron energy spectrum. A similar comparison can be made for the $^{33}\text{Al} \leftrightarrow ^{33}\text{Mg}$ pair in the same figure.

The introduction of magnetic fields can also create Urca pairs where they would not have otherwise existed. This is shown in Figure 4, for two pairs at densities and temperatures not conducive to the formation of Urca pairs for the nuclei shown at low fields. However, as the field increases, the rates can match and possibly form Urca pairs. The

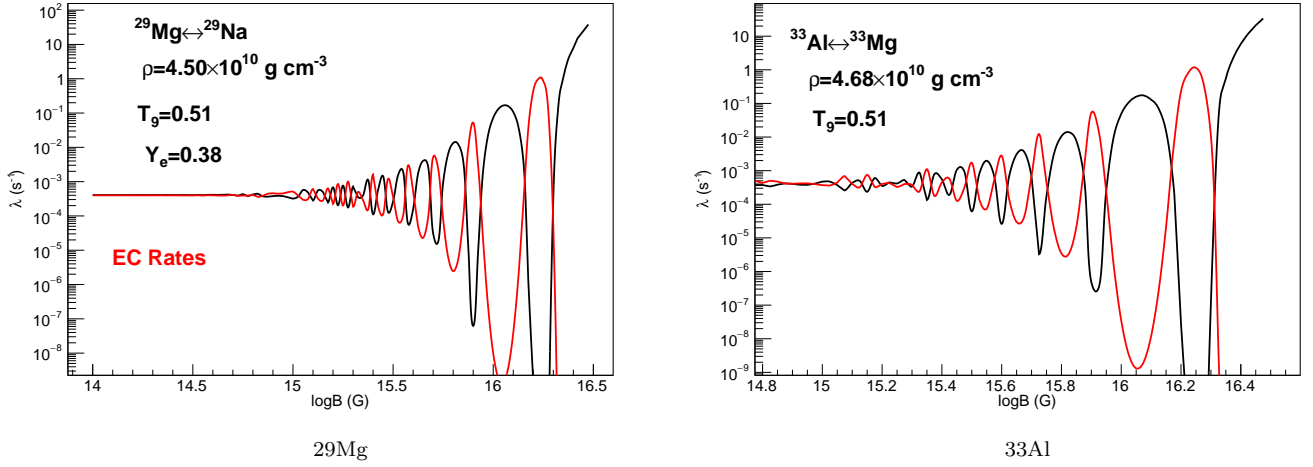


Figure 3. Examples of EC and β^- decay rates as a function of magnetic field for $^{29}\text{Mg} \leftrightarrow ^{29}\text{Na}$ (left) and $^{33}\text{Al} \leftrightarrow ^{33}\text{Mg}$ (right). The red line corresponds to the EC rate, while black lines correspond to the β^- rate.

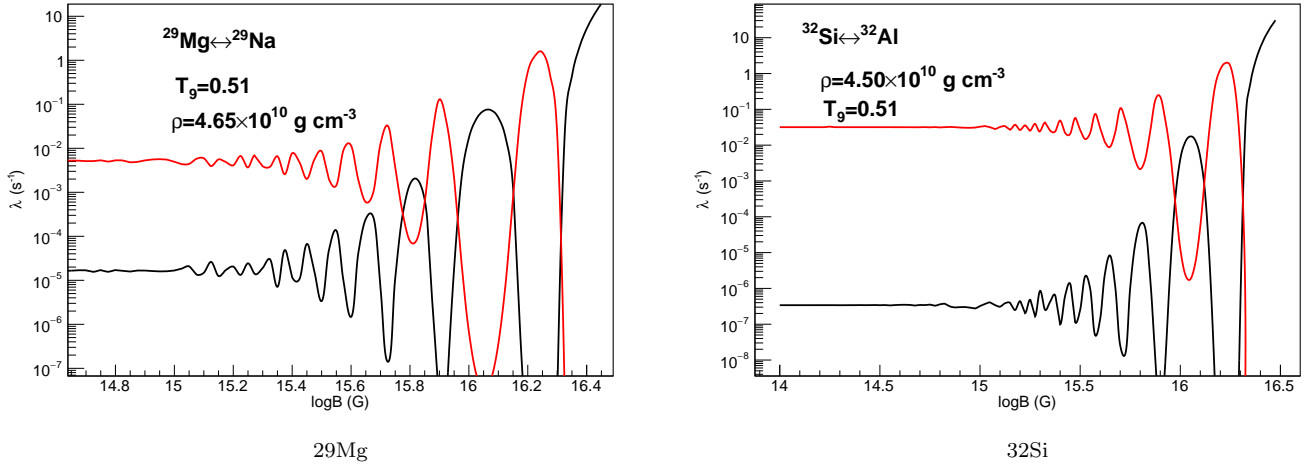


Figure 4. Evolution of Urca pair formation for $^{29}\text{Mg} \leftrightarrow ^{29}\text{Na}$ (left) and $^{32}\text{Si} \leftrightarrow ^{32}\text{Al}$ (right) at the indicated temperatures and densities.

additional degree of freedom from the magnetic field extends the range of possible conditions at which Urca pairs can form within the NS crust.

Finally, in addition to beta decay, Urca pairs can form for EC daughter excited states. For excited states in the EC daughter nucleus, the EC rate drops. The daughter nucleus de-excites almost immediately and decays via β^- decay back to the original nucleus. However, because the β^- rate exceeds the EC rate for excited states, the cooling efficiency is lower. The rate oscillations, however, may open Urca pair transitions to excited states in the EC daughter nucleus. This is shown in Figure 5. EC and β^- rates to the ground state of ^{31}Mg are shown as a function of magnetic field, as well as to the first two excited states of ^{31}Mg . While Urca pairs including excited states may not be possible at low field strength, higher fields may allow for Urca pairs between excited states. This is particularly interesting because EC to excited states may open up transition rates that are more favored.

As an example, Figure 6 shows the electron chemical potential as a function of polar angle for a layer of constant density and temperature within the crust. For all panels in this figure, a typical temperature of $T_9 = 0.51$ is adopted. For the top row of panels, $\rho Y_e = 4.70 \times 10^{10} \text{ g cm}^{-3}$, and for the bottom row $\rho Y_e = 3.73 \times 10^{10} \text{ g cm}^{-3}$.

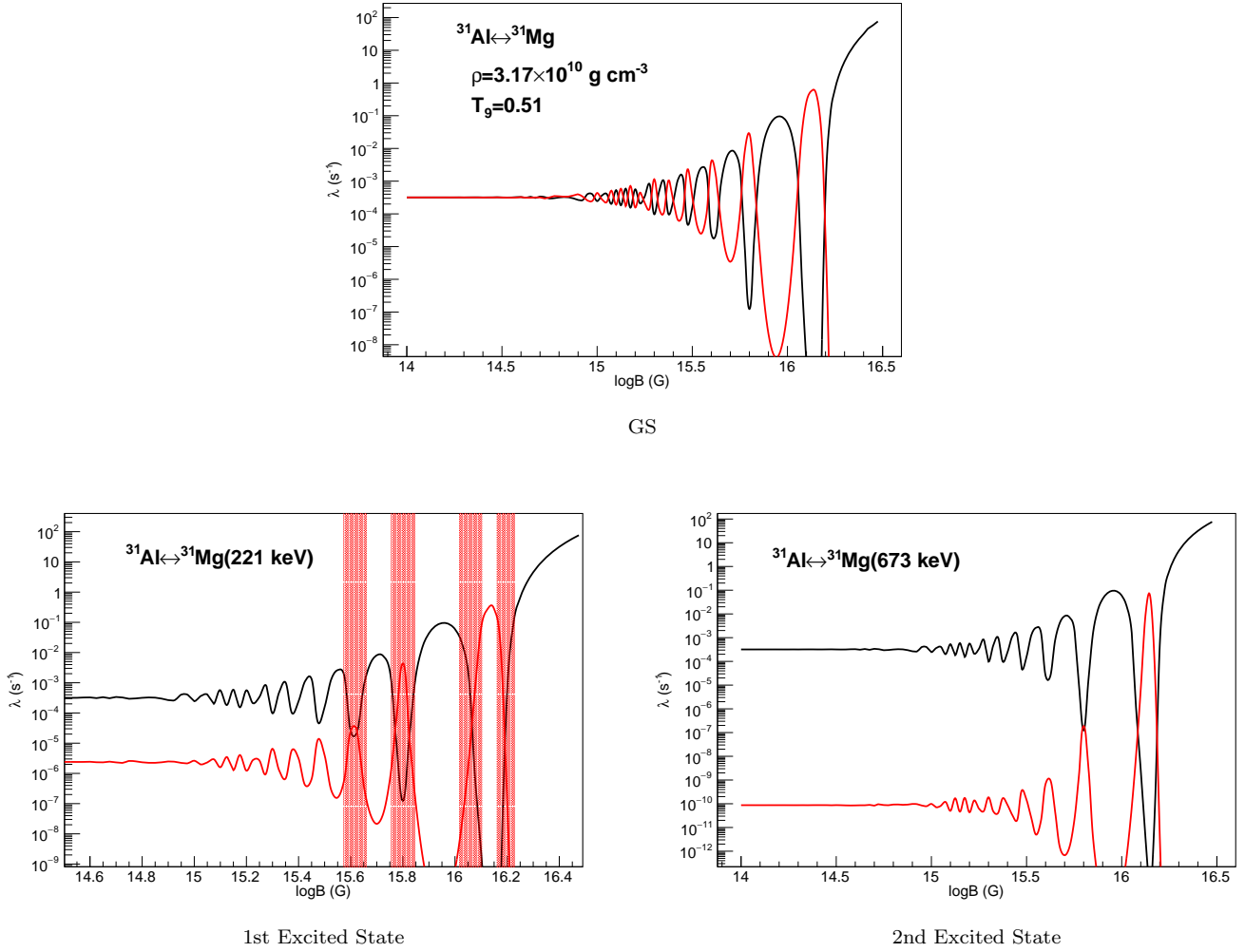


Figure 5. EC and β^- rates for the $^{31}\text{Al} \leftrightarrow ^{31}\text{Mg}$ Urca pair for transitions to the ground state in ^{31}Mg (top), the first excited state (bottom left), and the second excited state (bottom right). The red bands in the bottom left panel indicate fields where Urca pairing may be more efficient.

The shaded regions in these figures indicate those for which the chemical potential is within kT of the EC Q-values of the indicated reactions, $Q_{EC} - kT \leq \mu_e \leq Q_{EC} + kT$. With this evaluation, an Urca pair is not consistent across the entire surface of the NS at a given temperature and density. At high enough magnetic fields, an Urca pair may dominate a particular angular band. This may also have the effect of making additional Urca pairs possible in various angular regions.

Because of the shift in electron chemical potential with magnetic field, the location of Urca pairs within the neutron star crust varies with field and latitude (polar angle on the stellar surface). As an example, consider Figure 7, which shows the electron chemical potential as a function of polar angle for various surface magnetic fields (at the poles), latitudes, and densities within a NS crust. Because the chemical potential changes with both field and density, the physical location of Urca pairs may change. This will also result in a differentiation in the neutrino luminosity of various stars. For example, for a very large field of $10^{16.5}$ G as indicated in the figure, the density for which an Urca pair occurs is highest at the poles of the star, resulting in a larger polar neutrino luminosity, whereas, the stellar equator will form Urca pairs at a lower density. However, for the $^{63}\text{Cr} \leftrightarrow ^{63}\text{V}$ Urca pair, it can be seen that the minimum luminosity occurs at $\theta \approx 1.2$ rad. The magnetic field can result in a shift in the locations of Urca pairs as a function of latitude as seen in this figure. It can also be seen that magnetic fields will enable the existence of new pairs.

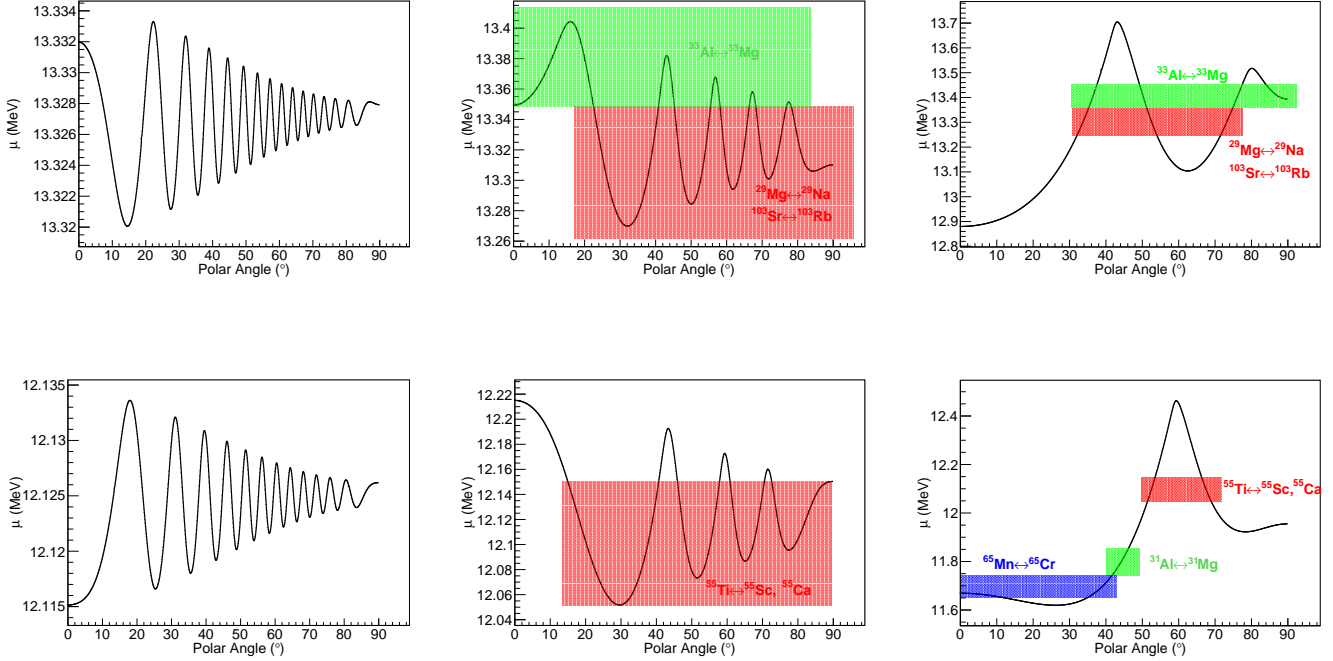


Figure 6. Prevalence of Urca pairs for two different values of ρY_e at various magnetic fields. Top row: $\rho Y_e = 1.7 \times 10^{10} \text{ g cm}^{-3}$, Bottom row: $\rho Y_e = 1.3 \times 10^{10} \text{ g cm}^{-3}$. Values are shown for magnetic fields of 10^{15} G (left), $10^{15.5} \text{ G}$ (center), and 10^{16} G . Shaded regions are regions where the indicated Urca pair dominates. For the left column, the dominant Urca pair is $^{29}\text{Mg} \leftrightarrow ^{29}\text{Na}$ and $^{103}\text{Sr} \leftrightarrow ^{103}\text{Rb}$ (top) and $^{55}\text{Ti} \leftrightarrow ^{55}\text{Ca}$, ^{55}Ca (bottom).

For a constant density and temperature, changes in magnetic field can result in a change in the electron chemical potential (Equation 1). This changes the overall phase space for electrons in β^- decay and electron capture. If an Urca pair is defined as a β^- -EC pair for which $\mu_e \sim Q$, then the density at which an Urca pair can exist also depends on the environmental magnetic field.

For example, the crusts and oceans of neutron stars have been modeled for various dipole fields defined by the field at the NS polar region. The density at which various Urca pairs are viable for various polar fields is shown in Figure 8 as a function of polar angle on the NS surface. For an assumed dipole field, the field is dependent on the NS polar angle at the surface. A 12 km diameter star with $M=1.4 M_\odot$ was considered. A constant temperature and Y_e of $T_9 = 0.51$ and $Y_e=0.41$ are assumed in each case. For these fixed parameters and a fixed dipole field, the density at which $\mu_e \sim Q$ is found. This is plotted in the left column of Figure 8 for fields of $B(\theta = 0)$ of 10^{14} G , 10^{15} G , and 10^{16} G . Because the field is not constant across the NS surface, the electron chemical potential is not constant for constant density.

Using the densities computed in Figure 8 (left panels), the neutrino emissivity as a function of polar angle in the NS ocean is plotted in the same figure (center). Here, the emissivity is normalized to the mass fraction of the relevant nuclei in these panels, ε/X . The emissivity is computed using the approximation of Deibel et al. (2016). Because we are interested in bulk behaviors of the neutrino emissivity and luminosity, we adopt the approximate weak rates of Arcones et al. (2010) using the phase space extracted from Equation 1 (Famiano et al. 2020). However, given the extraction of the ft values from the rates presumed in Deibel et al. (2016), the rate ratios given by the phase space differences with and without the magnetic fields, $\lambda(B \neq 0)/\lambda(B = 0)$ are expected to be independent of any nuclear structure effects in this evaluation.

The luminosity, L_{32} is shown on the right side of Figure 8 assuming an axisymmetric field for polar angle increments of $\Delta\theta = \pi/200$ radians. The radial thickness of each zone is calculated using the formulation of Schatz et al. (2014). For this calculation, a temperature of $T_9=0.51$, an electron fraction of $Y_e = 0.41$, a crust radius of 12 km, and a local gravity of $g = 1.85 \times 10^{14} \text{ cm s}^{-2}$ are assumed. The smaller overall solid angle near the poles results in an

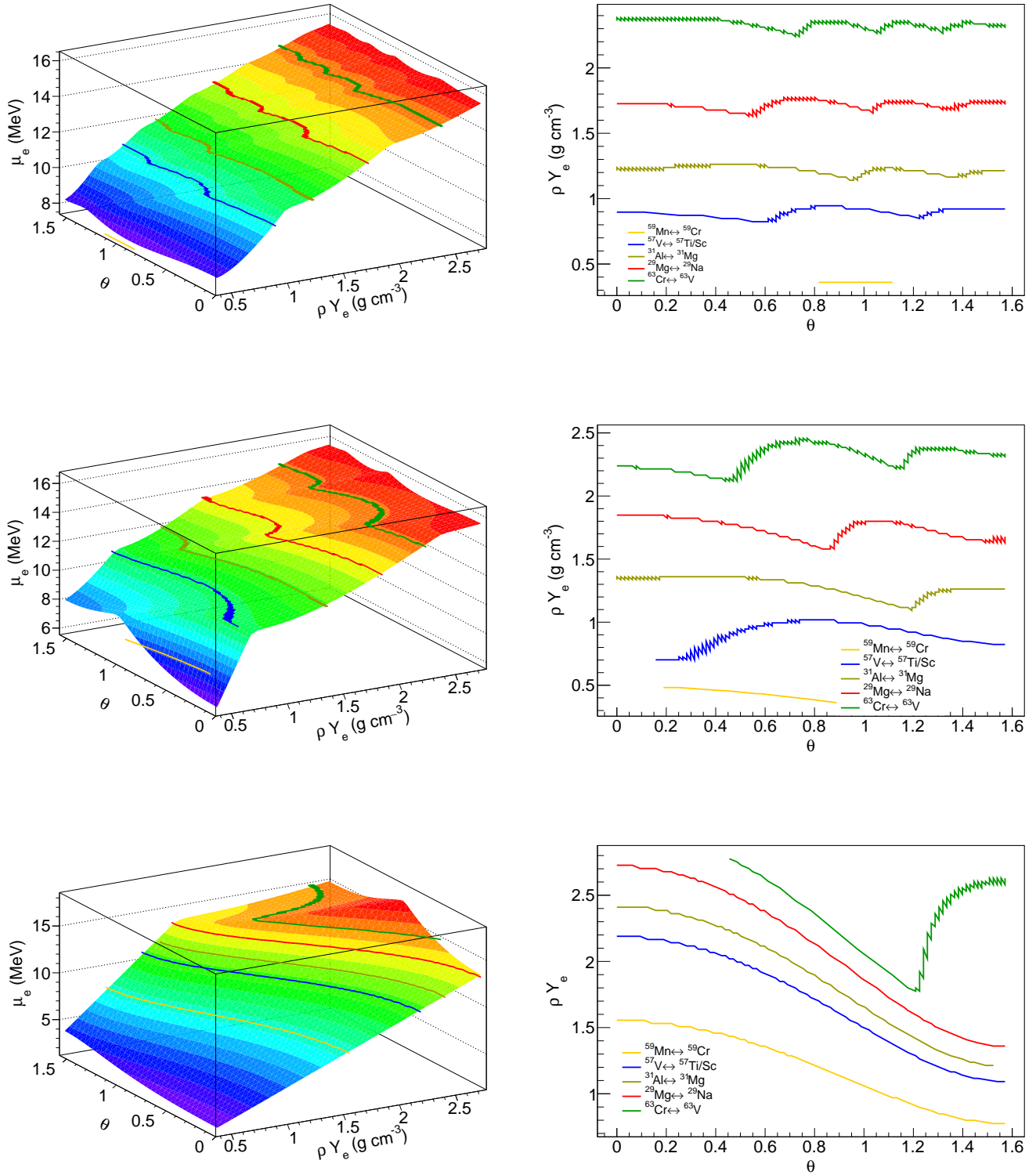


Figure 7. Left: Electron chemical potential as a function of ρY_e and polar angle for a neutron star with a dipole field of $10^{15.75} \text{ G}$ (top), 10^{16} G (middle), and $10^{16.5} \text{ G}$ (bottom). Units of ρY_e are $10^{10} \text{ g cm}^{-3}$. Right: The electron density ρY_e and polar angle for the same magnetic fields at which various crustal Urca pairs are present. These correspond to the lines in the left column.

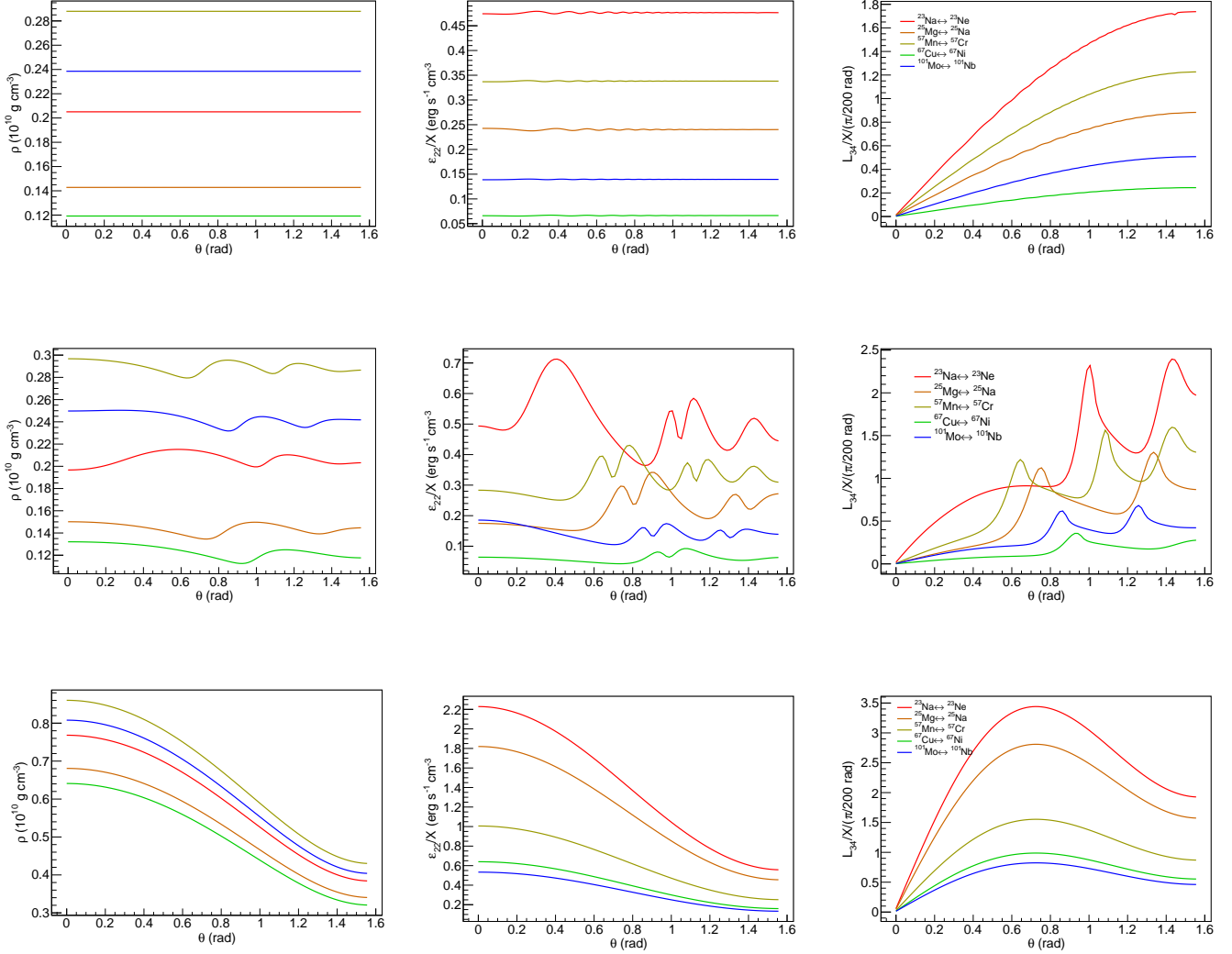


Figure 8. Left panels: The density at which an Urca pair is viable for various ocean Urca pairs. Center panels: The emissivity, ϵ_{22} , for various Urca pairs normalized to the mass fraction of the parent nucleus. Right panels: The luminosity, L_{34} , per angular bin for a bin size of $\pi/200$ rad for each Urca pair. The top, middle, and bottom rows correspond to a field B of 10^{14} G, 10^{15} G, and 10^{16} G respectively.

overall reduction of the total luminosity, though the emissivity may be larger in this region. The value of the neutrino emissivity, ϵ , is proportional to the weak interaction rates and is computed following the prescription of (Deibel et al. 2016).

There are multiple effects contributing to the behavior of the neutrino luminosity as a function of field. At the densities necessary for an Urca pair to exist, only the high(low)-energy tail of the electron energy spectrum is relevant for β^- (EC) decay. Also, a change in the local magnetic field will shift the overall electron chemical potential as shown in Figure 6. In this case, shifting the electron chemical potential in one direction or the other will result in a shift in the electron phase space, resulting in β decays or electron captures being impossible. As the magnetic field increases, the overlap between the Landau level distribution, the Fermi distribution, and the electron momentum space can interfere constructively or destructively, resulting in dramatic shifts in the optimum density at which an Urca pair can exist and changing the overall emissivities. This will be discussed below.

In this figure one can see that, for very high fields ($\sqrt{eB} \gtrsim Q$), the entire electron energy spectrum is confined to a single Landau level. As the field increases near the poles, the electron chemical potential decreases, resulting in a

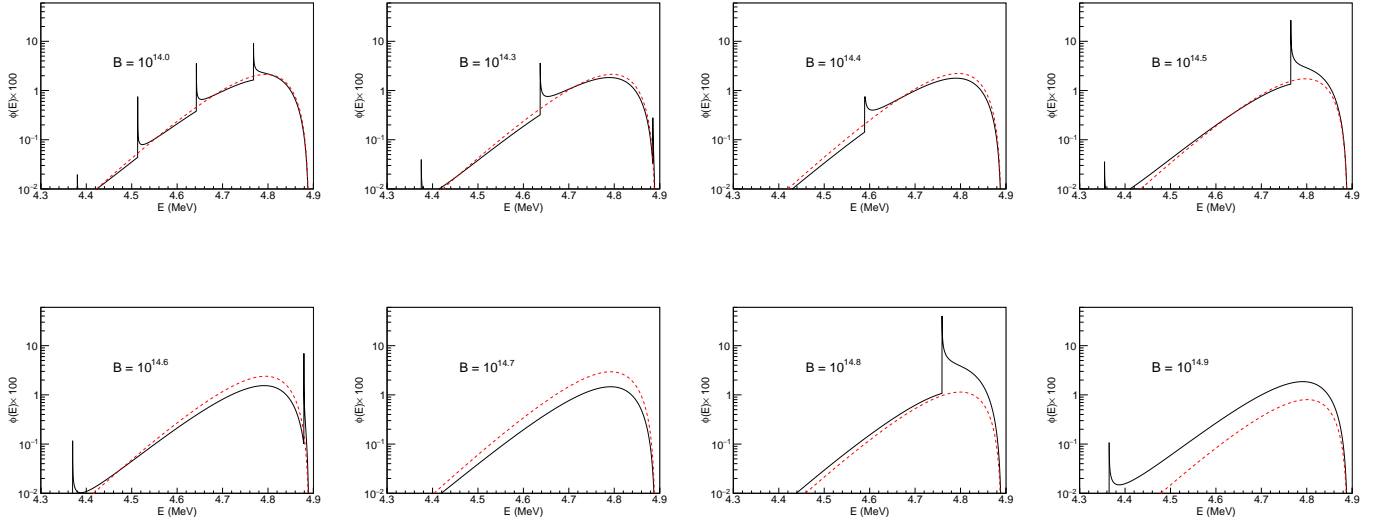


Figure 9. β^- Decay energy spectrum for various magnetic fields (G) for the ^{23}Ne decay. Red dashed lines correspond to the spectrum for $B=0$, and the solid black lines correspond to the spectrum for the fields indicated in each panel. Each plot in this figure is calculated at $T_9=0.51$, $Y_e=0.41$, and a density at which $\mu_e = Q_\beta$.

lower density at which an Urca pair can exist. This can result in a reduced emissivity. In addition, as the Landau level spacing increases, and the tail of the lowest Landau level ($E = m_e$) is more prominent in the electron energy spectrum. As the field decreases, and the Landau levels move closer together (but with a level spacing still greater than the Q value), the tail of the lowest Landau level becomes less prominent in the electron spectrum, resulting in a decrease in the overall rates.

For a very low field, $\sqrt{eB} \ll Q$, the effects of the Landau level spacing on the overall electron spectrum are minimal. Here, any change in field along the surface of the NS has little or no effect on the electron chemical potential, and the optimal density for an Urca pair does not change significantly.

The “intermediate field” regime ($\sqrt{eB} \sim Q$) is particularly interesting as the interference between the Landau level distribution and the Fermi distribution becomes prominent. In this regime, a small shift in the magnetic field can result in a shift in the optimum density of an Urca pair through a shift in the electron chemical potential. This contributes to a shift in the emissivity. Because the location of Landau levels strongly affects the availability of electrons to decay or capture, the effect can be magnified.

This can be seen in Figure 9, which shows the electron phase space distribution for ^{23}Ne decay in the $^{23}\text{Na} \leftrightarrow ^{23}\text{Ne}$ Urca pair. In each panel in this figure, the optimum density for this Urca pair to exist is computed (i.e., $\mu_e = Q_\beta$), and the resulting electron phase space spectrum (the integrand in the classical decay rate integral) is shown.

For a low field of 10^{14} G, the Landau level spacing is slightly less than the energy range of available electrons. As the field changes, the Landau level spacing changes, as do the positions of individual Landau levels. One sees that as the field increases above 10^{14} G, Landau levels can change location with respect to the edge of the Fermi distribution. At $10^{14.5}$ G, a Landau level exists at the right edge of the Fermi distribution with a less-prominent contribution from a level near 4.4 MeV. Most of the energy spectrum is dominated by the tail of the lower-energy Landau level. At a field of $10^{14.7}$ G, the Landau level spacing is larger than the available phase space created by the Fermi distribution and the electron momentum distribution. For this reason, much of the available electron energy spectrum is dominated by the tail of a low-energy Landau level. As the field increases towards 10^{15} G, the degeneracy of available Landau levels increases as electrons are placed in only the lowest few Landau levels, and the occupancy of the tails of the distributions becomes more important in the electron energy spectrum. When the field is high enough such that only the lowest Landau level is occupied, the tail of the distribution becomes quite prominent, and the electron energy spectrum is dominated by the single Landau level.

4. CONCLUSIONS

We explored the dependence and evolution of Urca pairs in crusts and oceans of magnetized neutron stars. Because the electron chemical potential depends on the environmental magnetic field, the presence or absence of Urca pairs must also depend on the external field. Urca pairs which may exist at a certain temperature and density, ρY_e , at zero magnetic field may not exist for a non-zero field. Conversely, Urca pairs which do not exist at specific temperatures and densities may appear in the presence of an external field. The presence of a magnetic field may also make excited states available in EC- β^- pairs. In this case, two nuclei which may not transition to low-lying states, may undergo transitions to excited states in the presence of an external field.

We also explored the evolution of Urca pairs along the surface of a magnetized neutron star. While we have assumed a dipole field for simplicity, this is sufficient to convey the concept that the variations in the field on the surface of a NS may change Urca pair locations within the crust/ocean of the star. Here, we have calculated the density at which an Urca pair may exist in a NS crust/ocean for a constant crust temperature of $T_9 = 0.51$. Of course, we note that the temperature of the crust varies with depth, so we acknowledge the simplification in this evaluation. This variation in density will result in a change in the neutrino emissivity and subsequent luminosity as a function of polar angle. We find that the emissivity (normalized to the mass fraction of the Urca pair studied) subsequently depends on the NS latitude, resulting in changes in the luminosity as a function of latitude.

However, because the density at which an Urca pair may exist in a NS is not constant, this ultimately affects the actual presence of an Urca pair at a location in a NS. This is because the density and the mass fraction changes with depth in the NS crust. At one location on the NS surface, an Urca pair may exist at one density while it exists at a different density at another location in the NS. However, the mass fractions of the Urca pair also vary at different densities/radii. For this reason, the emissivity is presented as normalized to the mass fraction, and a true computation of the emissivity must be multiplied by the mass fraction for the radius at which a specific density exists. Figure 8 can be used to scale Urca pair emissivity as a function of latitude for a known mass fraction, X . Thus, the emissivity can be expressed as a functional, $\epsilon = \epsilon(T, \rho Y_e, B, X) = \epsilon(T, \rho(r, \theta) Y_e(r), B(\theta)) = \epsilon(T, r, \theta, B_0)$, where B_0 is the magnetic field at the NS pole.

It may very well be possible that the mass fraction in the region at which an Urca pair may be viable is zero, while it is non-zero in another viable region. Thus, an Urca pair may exist in one part of the NS, but not in another. We have shown that the addition of a magnetic field to NS luminosity calculations adds another layer of complexity to the total emissivity calculation, and ultimately may result in uneven NS cooling along the surface of the star.

There may be several ramifications of this result which will be explored in subsequent papers. First, we find that the bulk luminosity of a NS is dependent on its magnetic field. This can ultimately change the cooling curve of the star. Perhaps variations in NS luminosities are a result of the surface field. Likewise, limits can be placed on NS surface fields from observations of their cooling.

Second, uneven neutrino emissivity on the NS surface can result in uneven cooling and heating in the crust. This can have affect the thermal equation of state on the surface and may be a way of explaining NS crust quakes or possibly even NS kicks.

Certainly, an exhaustive treatment of the overall complexity of this problem is beyond the scope of the present work. More precise work is needed. In particular, a thorough evaluation of the presence or absence of Urca pairs as a function of density, temperature, and magnetic field is needed. From this, luminosity maps can be produced for NSs with various field configurations. In order to produce these, realistic models of ocean/crust abundances can be developed. While these will be explored in future work, our current results introduce the possibility that magnetized neutron stars may have uneven cooling as a result of variations in the interior magnetic field, and the overall bulk luminosity changes with the field configuration and magnitude.

REFERENCES

- Arcones, A., Martínez-Pinedo, G., Roberts, L. F., & Woosley, S. E. 2010, *A&A*, 522, A25, doi: [10.1051/0004-6361/201014276](https://doi.org/10.1051/0004-6361/201014276)
- Boguta, J. 1981, *Physics Letters B*, 106, 255, doi: [10.1016/0370-2693\(81\)90529-3](https://doi.org/10.1016/0370-2693(81)90529-3)
- Chanmugam, G. 1992, *ARA&A*, 30, 143, doi: [10.1146/annurev.aa.30.090192.001043](https://doi.org/10.1146/annurev.aa.30.090192.001043)
- Deibel, A., Meisel, Z., Schatz, H., Brown, E. F., & Cumming, A. 2016, *ApJ*, 831, 13, doi: [10.3847/0004-637X/831/1/13](https://doi.org/10.3847/0004-637X/831/1/13)
- Famiano, M., Balantekin, A. B., Kajino, T., et al. 2020, *ApJ*, 898, 163, doi: [10.3847/1538-4357/aba04d](https://doi.org/10.3847/1538-4357/aba04d)
- Fassio-Canuto, L. 1969, *Physical Review*, 187, 2141, doi: [10.1103/PhysRev.187.2141](https://doi.org/10.1103/PhysRev.187.2141)

- Grasso, D., & Rubinstein, H. R. 2001, *PhR*, 348, 163, doi: [10.1016/S0370-1573\(00\)00110-1](https://doi.org/10.1016/S0370-1573(00)00110-1)
- Haensel, P., & Gnedin, O. Y. 1994, *A&A*, 290, 458
- Jones, S., Hirschi, R., Nomoto, K., et al. 2013, *ApJ*, 772, 150, doi: [10.1088/0004-637X/772/2/150](https://doi.org/10.1088/0004-637X/772/2/150)
- Kawasaki, M., & Kusakabe, M. 2012, *PhRvD*, 86, 063003, doi: [10.1103/PhysRevD.86.063003](https://doi.org/10.1103/PhysRevD.86.063003)
- Kouveliotou, C., Dieters, S., Strohmayer, T., et al. 1998, *Nature*, 393, 235, doi: [10.1038/30410](https://doi.org/10.1038/30410)
- Lai, D., Abrahams, A. M., & Shapiro, S. L. 1991, *ApJ*, 377, 612, doi: [10.1086/170389](https://doi.org/10.1086/170389)
- Lattimer, J. M., Pethick, C. J., Prakash, M., & Haensel, P. 1991, *PhRvL*, 66, 2701, doi: [10.1103/PhysRevLett.66.2701](https://doi.org/10.1103/PhysRevLett.66.2701)
- Luo, Y., Famiano, M. A., Kajino, T., Kusakabe, M., & Balantekin, A. B. 2020, *PhRvD*, 101, 083010, doi: [10.1103/PhysRevD.101.083010](https://doi.org/10.1103/PhysRevD.101.083010)
- Maruyama, T., Balantekin, A. B., Cheoun, M.-K., et al. 2022, *Physics Letters B*, 824, 136813, doi: [10.1016/j.physletb.2021.136813](https://doi.org/10.1016/j.physletb.2021.136813)
- Mori, K., Famiano, M. A., Kajino, T., Kusakabe, M., & Tang, X. 2019, *MNRAS*, 482, L70, doi: [10.1093/mnrasl/sly188](https://doi.org/10.1093/mnrasl/sly188)
- Paczyński, B. 1972, *Astrophys. Lett.*, 11, 53
- Schatz, H., Gupta, S., Möller, P., et al. 2014, *Nature*, 505, 62, doi: [10.1038/nature12757](https://doi.org/10.1038/nature12757)
- Tsuruta, S., & Cameron, A. G. W. 1970, *Ap&SS*, 7, 374, doi: [10.1007/BF00653278](https://doi.org/10.1007/BF00653278)
- Turolla, R., Zane, S., & Watts, A. L. 2015, *Reports on Progress in Physics*, 78, 116901, doi: [10.1088/0034-4885/78/11/116901](https://doi.org/10.1088/0034-4885/78/11/116901)
- Woosley, S. E., & Weaver, T. A. 1986, *ARA&A*, 24, 205, doi: [10.1146/annurev.aa.24.090186.001225](https://doi.org/10.1146/annurev.aa.24.090186.001225)
- Yakovlev, D. G., Kaminker, A. D., Gnedin, O. Y., & Haensel, P. 2001, *PhR*, 354, 1, doi: [10.1016/S0370-1573\(00\)00131-9](https://doi.org/10.1016/S0370-1573(00)00131-9)
- Yakovlev, D. G., & Levenfish, K. P. 1995, *A&A*, 297, 717

T.K. is supported in part by Grants-in-Aid for Scientific Research of JSPS (17K05459, 20K03958). A.B.B. is supported in part by the U.S. National Science Foundation Grants No. PHY-2020275 and PHY-2108339. M.A.F. is supported by National Science Foundation Grant No. PHY-1712832 and by NASA Grant No. 80NSSC20K0498. K.M. is supported by Research Institute of Stellar Explosive Phenomena at Fukuoka University and JSPS KAKENHI Grant Number JP21K20369. M.A.F., G.J.M. and A.B.B. acknowledge support from the NAOJ Visiting Professor program. Work at the University of Notre Dame (G.J.M.) supported by DOE nuclear theory grant DE-FG02-95-ER40934.